Bioorganic & Medicinal Chemistry Letters xxx (2014) xxx–xxx

Contents lists available at ScienceDirect

Bioorganic & Medicinal Chemistry Letters

journal homepage: www.elsevier.com/locate/bmcl

Structure activity relationships of human galactokinase inhibitors

Li Liu [a], Manshu Tang [b], Martin J. Walsh [a,†], Kyle R. Brimacombe [a], Rajan Pragani [a], Cordelle Tanega [a], Jason M. Rohde [a], Heather L. Baker [a], Elizabeth Fernandez [a], Burchelle Blackman [a,‡], James M. Bougie [a], William H. Leister [a], Douglas S. Auld [a,§], Min Shen [a], Kent Lai [b], Matthew B. Boxer [a,*]

[a] National Center for Advancing Translational Sciences, National Institutes of Health, 9800 Medical Center Drive, Rockville, MD 20850, USA
[b] Division of Medical Genetics, Department of Pediatrics, University of Utah, Rm 2C412 SOM, 50 N. Medical Drive, Salt Lake City, UT 84132, USA

ARTICLE INFO

Article history:
Received 22 October 2014
Revised 19 November 2014
Accepted 21 November 2014
Available online xxxx

Keywords:
Galactosemia
Structure–activity relationships
Galactokinase

ABSTRACT

Classic Galactosemia is a rare inborn error of metabolism that is caused by deficiency of galactose-1-phosphate uridyltransferase (GALT), an enzyme within the Leloir pathway that is responsible for the conversion of galactose-1-phosphate (gal-1-p) and UDP-glucose to glucose-1-phosphate and UDP-galactose. This deficiency results in elevated intracellular concentrations of its substrate, gal-1-p, and this increased concentration is believed to be the major pathogenic mechanism in Classic Galactosemia. Galactokinase (GALK) is an upstream enzyme of GALT in the Leloir pathway and is responsible for conversion of galactose and ATP to gal-1-p and ADP. Therefore, it was hypothesized that the identification of a small-molecule inhibitor of human GALK would act to prevent the accumulation of gal-1-p and offer a novel entry therapy for this disorder. Herein we describe a quantitative high-throughput screening campaign that identified a single chemotype that was optimized and validated as a GALK inhibitor.

Published by Elsevier Ltd.

The galactosemias are rare inherited metabolic disorders caused by deficiencies of the enzymes in the Leloir Pathway.[1,2] As the Leloir Pathway is the predominate mechanism for the metabolism of galactose, all of the galactosemias result in aberrant levels of galactose and/or its down-stream metabolites (Fig. 1). Classic Galactosemia (Type I) is the most common form of the galactosemias and is also the most severe. It is a potentially lethal disorder with a high mortality rate when left untreated. Currently, many state newborn screening programs include testing for galactosemia, and if detected, immediate removal of lactose and galactose from an infant's diet is required.[3] With widespread incorporation of this screening, the morbidity rates for those affected with Classic Galactosemia has significantly decreased, but the life-long galactose restricted diet fails to prevent developmental delay, neurological disorders, and premature ovarian insufficiency, which occur in many affected patients later in life.[4–7] Classic Galactosemia is characterized by deficient galactose-1-phosphate uridyltransferase (GALT), which results in the buildup of its substrate galactose-1-phosphate (gal-1-P).[8] Although the exact pathogenic mechanism of Classic Galactosemia has not been established, elevated galactose-1-phosphate (gal-1-p) levels have been proposed as a major pathogenic factor.[3,9–11] Immediately upstream from GALT is galactokinase (GALK), which is the enzyme responsible for converting galactose into gal-1-p. Deficiency in the GALK enzyme results in Type II Galactosemia and these GALK-deficient patients have much milder and even benign phenotypes.[12] This positions GALK as a target for reduction of gal-1-p levels and a potential therapeutic target for Classic Galactosemia.[13,14]

Using recombinant GALK1 we performed a quantitative high-throughput screen (qHTS) against ~274,000 compounds in 1536-well plate format at 6 doses (3 nM–57 μM).[13,15] ATP was held at 35 μM and galactose at 100 μM, both near their K_m values determined under the 1536-well assay conditions. We used the KinaseGlo™ detection system, which measures remaining ATP levels after conversion of galactose to gal-1p by GALK1. While the screen performed acceptably ($Z' = 0.48 \pm 0.16$, signal/background = 4.5 ± 1.6 and CV = 17 ± 9), there was an extremely low initial hit rate of 0.05%. Counter-screens were run to identify potential false positives with activity against the KinaseGlo detection reagent itself in ATP containing buffer; and with interfering redox activity, as measured by H_2O_2 production in an HRP-phenol red coupled assay (PubChem AIDs 1379 and 2502, respectively). With the exclusion of these two classes of potential artifacts only 65

* Corresponding author. Tel.: +1 301 217 4681; fax: +1 301 217 5736.
E-mail address: boxerm@mail.nih.gov (M.B. Boxer).
† Present address: Dow AgroSciences LLC, Crop-Protection Discovery, Group, Bldg. 306/E2/980, 9330 Zionsville Road, Indianapolis, IN 46268, USA.
‡ Present address: Imaging Probe Development Center, National Heart, Lung, and Blood Institute, National Institutes of Health, 9800 Medical Center Drive, Rockville, MD 20850, USA.
§ Present address: Center for Proteomic Chemistry, Novartis Institutes for Biomedical Research, Cambridge, MA 02139, USA.

http://dx.doi.org/10.1016/j.bmcl.2014.11.061
0960-894X/Published by Elsevier Ltd.

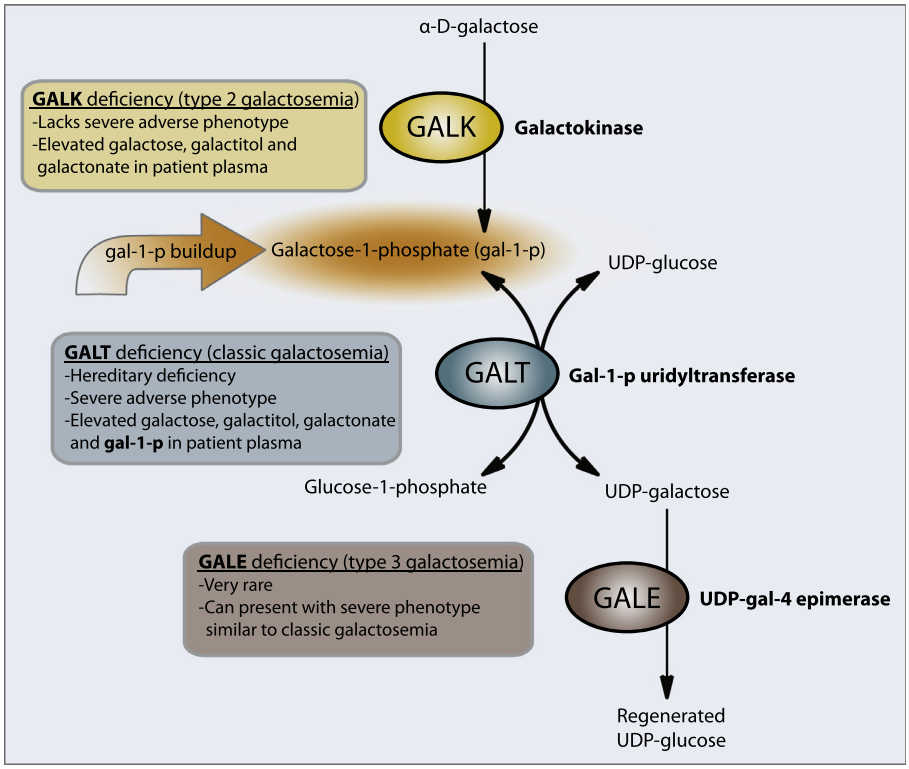

Figure 1. The Leloir pathway for galactose metabolism, highlighting the deficient enzymes responsible for the galactosemias.

compounds remained. Within this small list of compounds, the spiro-benzoxazole series, exemplified by **1** (PubChem CID 1286615), emerged as a validated hit series. Upon resynthesis of **1** using the one-pot procedure reported by Potapov et al. (Scheme 1),[16] we confirmed the GALK1 inhibitory activity with an IC_{50} of 6 μM and began initial structure activity relationship (SAR) exploration.

While the resynthesis of **1** performed well in refluxing isopropanol, the chemistry did not translate well to more diverse substrates. After unsuccessfully trying a few acid and base catalysts, we settled on mixing the three components neat, sealing in a microwave vial, and submerging into a 120 °C oil bath (Scheme 2). This protocol allowed for rapid access to a number of analogs for initial SAR (Table 1).

We first looked at the importance of the gem-dimethyl group and found that replacement with a mono-phenyl substituent (**2**) gave reduced activity, while complete removal of the methyl groups gave improved activity to 1 μM (**3**). Contracting the fused cyclohexenone ring to a 5-membered ring (**4**) reduced activity. Next, we looked at the spiro ring and made cyclohexane (**5**), dimethyl (**6**) and cyclobutane (**7**) analogs. While all three analogs maintained GALK1 inhibitory activity, they were significantly weaker than **3**. Attempts to replace the benzoxazole were limited by the chemistry in this multi-component reaction, but we were able to access two guanidinyl benzimidazoles (**8** and **9**) through chemistry outlined in Scheme 3, followed by the standard neat melting chemistry typified in Scheme 2. Unfortunately, both analogs were inactive. Due to the low solubility of **3** and with

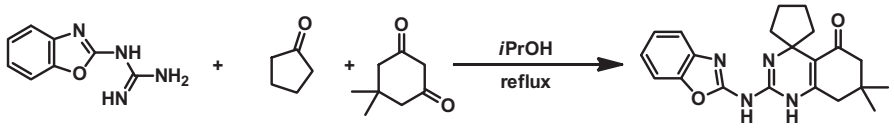

Scheme 1. Resynthesis of **1**.

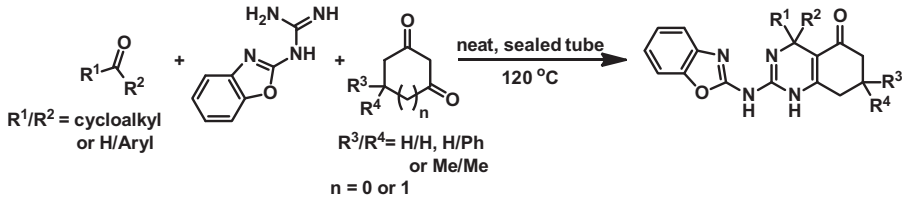

Scheme 2. Use of neat melting procedure for broader applicability to diverse substrates.

Table 1
Initial SAR around hit **1**

Compounds	Structure	IC_{50}[a] (μM)	Max response[b] (%)
1	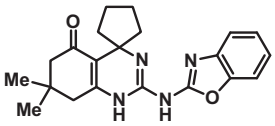	6.0	−82
2	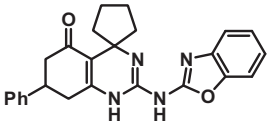	ND	−36
3	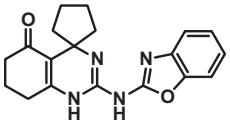	1.0	−86
4	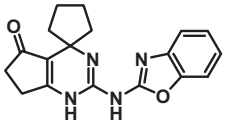	13.3	−75
5	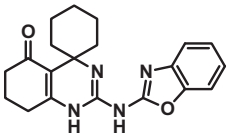	11.9	−99
6	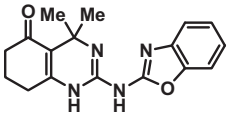	16.8	−74
7	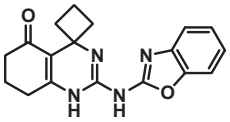	16.8	−74
8	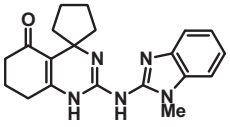	ND	<10
9	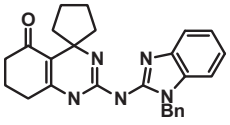	ND	<10

[a] IC_{50} values were determined utilizing the luminescence GALK-ATP-depletion assay. ND = not determined; for compounds with max response at 57 μM weaker than 50%, IC_{50} was ND.
[b] Max Resp. represents the % inhibition at 57 μM compound.

the realization that the chemistry enabled the use of non-enolizable aldehydes in the 3-component reaction, we synthesized analogs that replaced the alkyl-spiro substituent with aryl groups (Table 2).

While the phenyl analog (**10**) had GALK1 inhibitory activity, it was severely diminished compared to many of the spiro analogs in Table 1 (~25 fold less potent). A scan of *para* and *meta* substituents (**11**–**18**) resulted in very weak inhibitors showing minimal GALK inhibition at the top dose of 57 μM. Interestingly, *ortho* substituted phenyl analogs showed a preference for chloro (**19**), bromo (**21**) or CF_3 (**22**) groups, all of which gave IC_{50} values under 8 μM. The corresponding methoxy analog (**20**) showed weak inhibition. Combining two *ortho* chloro substituents (**23**), resulted in reduced potency. Pyridine and pyrazole analogs not bearing a 2-substituent had minimal activity (**24**–**26**).

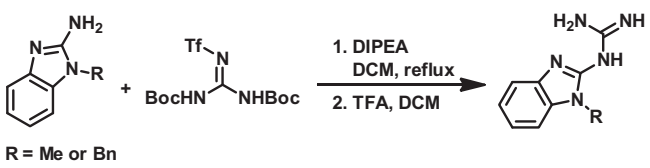

Scheme 3. Synthesis of benzimidazole-guanidines.

While there was a preference for *ortho*-halogenated analogs for reasonable potencies, these analogs all had aqueous solubilities of <1 μg/mL. In an effort to improve this property, we decided to investigate whether this motif could be combined with heterocyclic groups in hopes of obtaining improved compounds. To this end, we synthesized a variety of analogs utilizing 2-halogenated

Table 2
SAR around the aryl ring showing preference for *ortho*-substitution

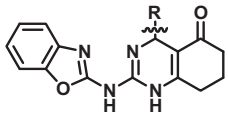

Compounds	R	IC_{50}[a] (μM)	Max response[b] (%)	Compounds	R	IC_{50}[a] (μM)	Max Response[b] (%)
10		25	−70	**19**	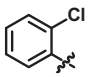	6	−77
11	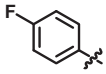	ND	−38	**20**	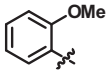	ND	−36
12	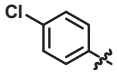	ND	−11	**21**	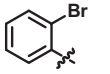	3	−84
13	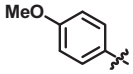	ND	−33	**22**	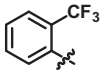	8	−79
14	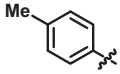	ND	−35	**23**	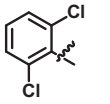	ND	−44
15	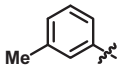	ND	−32	**24**		ND	−15
16	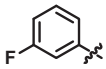	ND	−45	**25**		ND	−37
17	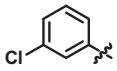	ND	−25	**26**		ND	−24
18	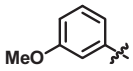	18.1	−60				

[a] IC_{50} values were determined utilizing the luminescence GALK-ATP-depletion assay. ND = not determined; for compounds with max response at 57 μM weaker than 50%, IC_{50} was ND.
[b] Max Resp. represents the % inhibition at 57 μM compound.

heterocyclic aldehyde starting materials (Table 3). 2-Chloro, -bromo and -trifluoromethyl pyridine isomers were made (**27**–**33**), with most giving potency in the range of ~3–10 μM, while the 2-halopyridin-3-yl analogs **28** and **29** were essentially inactive. Next, two bromo-pyrazoles (**34** and **35**) were synthesized, giving potencies of 5.7 and 4.2 μM, respectively. The corresponding chloro-pyrazoles (**36** and **37**) were 4.7 and 12.8 μM respectively, while the regioisomeric methyl-chloropyrazole (**38**) had no detectable inhibition. In an effort to both understand the effect of the *ortho*-substituent and confirm the structure of the product of the 3-component reaction, we crystallized **32** and obtained an X-ray structure (Fig. 2). The structure was confirmed and the presence of the *ortho*-trifluoromethyl group was shown to position the phenyl ring with a torsion angle of ~90° from the plane of the adjacent ring. It is surmised that this orientation is preferred for inhibition of GALK.

Being that a number of 2-halo substituted heterocycles (**27**, **31**, **34**, **35** and **36**) had similar potencies, we looked at a preliminary in vitro ADME profile (Table 4). While all analogs had good PAMPA permeability (>750 × 10^{-6} cm/s), they differed in kinetic aqueous solubility and rat liver microsomal stability (RLMS). The *ortho*-chloro pyridyl analog (**27**) had moderate solubility and poor RLMS, while the corresponding *ortho*-bromo analog (**31**) had low solubility and RLMS. The two bromo-pyrazole analogs (**34** and **35**) differed greatly in solubility, while the chloro-pyrazole analog (**36**) gave the best solubility and RLMS (32 μg/mL and 18 min half-life, respectively) with a concordantly high PAMPA permeability. We also determined that **36** was stable in PBS buffer (pH = 7.4) as well as in the presence of 5 mM glutathione, had moderate mouse liver microsomal stability ($t_{1/2}$ = 34 min) and good mouse plasma stability ($t_{1/2}$ >60 min) (Table 5). The compound was also stable to oxidants (air and MnO_2) indicating it was not redox active. Being that **36** had the best preliminary in vitro ADME profile, we decided to carry it on for further selectivity, mechanism of action and cell-based studies.

To determine the mode of inhibition for **36**, mechanistic substrate competition studies were performed by independently titrating both ATP and galactose substrates in a coupled GALK1 assay system. Analog **36** appeared to shift the K_m of ATP (Fig. 3A and B), suggesting that the compound is competitive with respect to ATP, an observation which was corroborated by mixed-model curvefits of the data (α = 2.035e17) and visualized using Lineweaver–Burk transformation of the kinetic data. Galactose, conversely, appeared to show changes in both K_m and V_{max} in the presence of **36**, suggestive of uncompetitive inhibition with respect to galactose (Fig. 3C and D). Mixed-model curve fitting yielded alpha values consistent with uncompetitive activity (α = 0.0007), suggesting that **36** may bind to the GALK1-galactose complex with greater affinity than the free enzyme itself. Taken together, these observations confirm that **36** directly competes with ATP at the binding site, and suggest that galactose may be required to bind first, prior to **36** binding and inhibition. Next, **36** was first profiled

Table 3
SAR of various *ortho*-substituted aryl groups

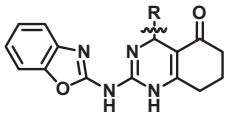

Compounds	R	IC_{50}[a] (μM)	Max response[b] (%)	Compounds	R	IC_{50}[a] (μM)	Max response[b] (%)
27		9.9	−82	**33**	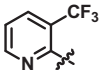	6.4	−61
28		ND	−47	**34**	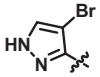	5.7	−85
29		ND	−39	**35**	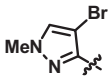	4.2	−86
30		4.9	−64	**36**	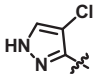	4.7	−86
31		3.1	−92	**37**	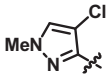	12.8	−70
32	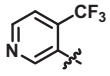	7.6	−64	**38**		ND	−14

[a] IC_{50} values were determined utilizing the luminescence GALK-ATP-depletion assay. ND = not determined; for compounds with max response at 57 μM weaker than 50%, IC_{50} was ND.
[b] Max Resp. represents the % inhibition at 57 μM compound.

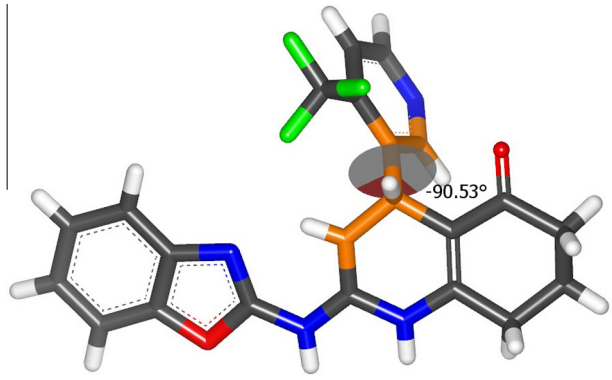

Figure 2. X-ray structure of **32**.

against human GALK2 (isozyme with 30% sequence identity to human GALK1 and 45% homology) and a large portion of the kinome using DiscoveRx's® Kinome Scan. Compound **36** showed no inhibition up to 40 μM for GALK2 (Fig. 4) and an extremely clean profile against the kinome (see Supplemental). This is likely due to the significant difference of the ATP binding sites for protein kinases compared to this GHMP small molecule kinase. The analogy between these two types of kinases is very low since the GALK1 active site lacks the typical components that almost all protein kinases share, such as the hinge region, glycine-rich loop and activation loop.

One of the major phenotypes of patients with Classic Galactosemia is very high gal-1-p levels in their red blood cells, fibroblasts and other tissue. With access to primary patient fibroblasts from the University of Utah, we looked for the ability of **36** to lower gal-1-p levels in these patient cells (Fig. 5). Glucose challenge

Table 4
Early ADME on select GALK1 inhibitors

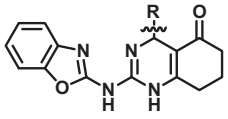

Compounds	R	RLMS[a,b] $t_{1/2}$ (min)	PAMPA[b] ($\times 10^{-6}$ cm/s)	Aq solubility[b,c] (μg/mL)
27		7	897	9
31		7	1515	<1
34	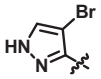	14	798	<1
35	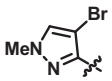	9	1351	25
36	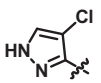	18	983	32

[a] RLMS = rat liver microsome stability.
[b] Performed in-house at NCATS.
[c] Kinetic aq solubility in PBS 7.4 buffer from a 10 mM DMSO compound stock solution.

resulted in a ratio of gal-1-p/protein of 12 ng/μg, while galactose challenge resulted in a ratio of 33 ng/μg. Upon pretreatment with compound followed by galactose challenge, **9**, our inactive control,

Table 5
Additional early ADME for **36**

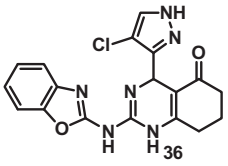

In vitro ADME	
PBS buffer (pH = 7.4) stability (% remaining after 48 h)	>95%
5 mM aqueous glutathione stability (% remaining after 48 h)	>95%
Mouse microsomal stability ($t_{1/2}$)	34 min
Mouse plasma stability ($t_{1/2}$)	>60 min

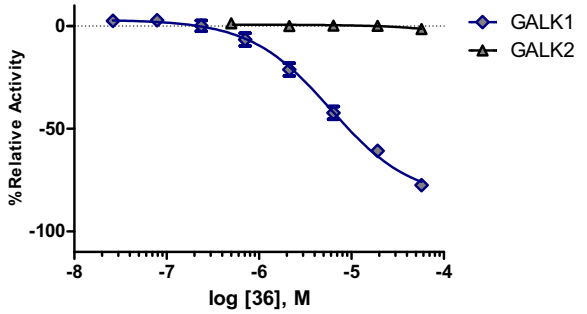

Figure 4. Dose–response curve for **36** assayed against GALK1 and GALK2.

gave no reduction in gal-1-p, while **36** gave a dose–response reduction and reduced levels below the glucose challenge level in this primary patient fibroblasts (Fig. 5A). Both **9** and **36** had no significant effect on viability of the patient fibroblasts as determined by total protein content (Fig. 5B).

In summary, following a qHTS campaign for inhibitors of GALK1, we optimized a spiro-benzoxazole-containing series to low micromolar potency with reasonable early ADME properties. SAR revealed that the spiro group, or a 2-substituted aryl group was required to maintain the activity. The use of 2-substituted heteroaryl groups was key to obtaining compounds with decent solubility, allowing for MOA studies that found this series to be ATP competitive. Analog **36** was assessed for its ability to lower gal-1-p in primary patient fibroblasts and gave a nice dose-response with no detrimental effect on cell viability. The compounds described herein should represent useful tools for studying galactose metabolism in general as well as understanding the role of GALK1 in Classic Galactosemia.

Acknowledgements

We thank Danielle van Leer, Misha Itkin, Crystal McKnight, Christopher LeClair and Paul Shinn for assistance with compound management. We also thank Arnold L. Rheingold and Curtis Moore at UCSD for X-ray determination of **32**. This research was supported by the Molecular Libraries Initiative of the National Institutes of Health Roadmap for Medical Research Grant U54MH084681 and the Intramural Research Program of the National Center for Advancing Translational Sciences at the National Institutes of Health. Research Grant support to K.L. include R03MH085689 and R01HD074844-2.

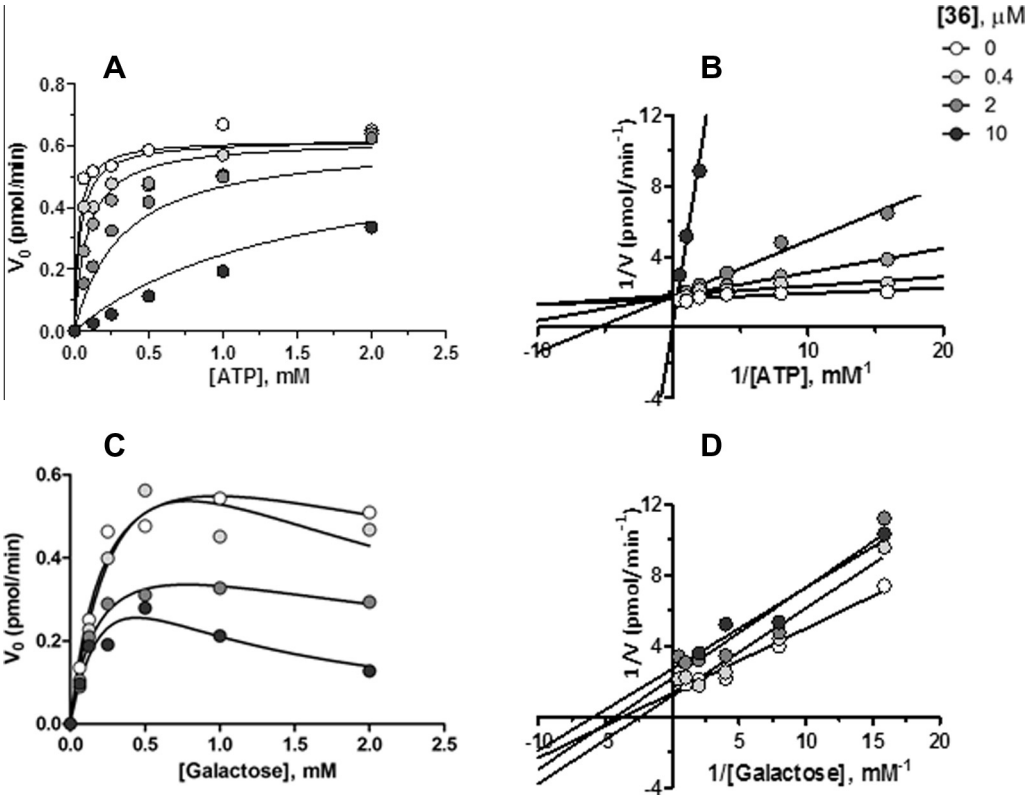

Figure 3. (A) Initial velocity plot of competition relationship between **36** and ATP; (B) Lineweaver–Burk transformation of **36**: ATP initial rates; (C) Initial velocity plot of competition relationship between **36** and galactose; (D) Lineweaver–Burk transformation of **36**: galactose initial rates.

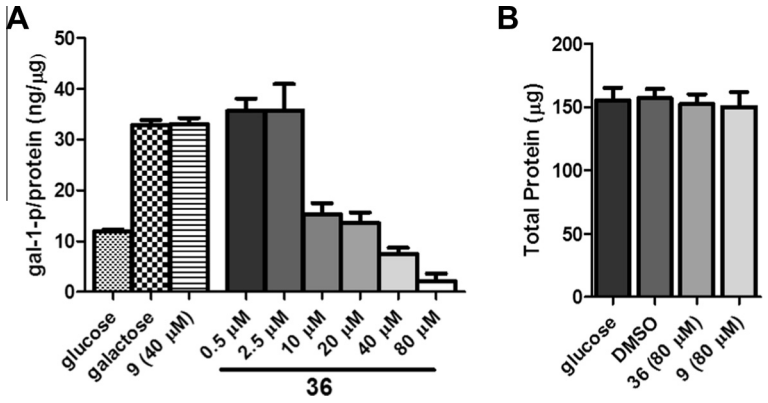

Figure 5. (A) Gal-1-p levels measured in primary galactosemic patient fibroblasts after either glucose, galactose and/or galactose and compound treatment regimes. (B) Total protein content after designated treatment in primary galactosemic patient fibroblasts.

Supplementary data

Supplementary data (synthetic procedures, selected analytical data, in vitro and cell-based experimental) associated with this article can be found, in the online version, at http://dx.doi.org/10.1016/j.bmcl.2014.11.061.

References and notes

1. Leloir, L. F. *Arch. Biochem. Biophys.* **1951**, *33*, 186.
2. Berry, G. T.; Walter, J. H. Disorders of Galactose Metabolism. In *Inborn Metabolic Diseases-Diagnosis and Treatment*; Fernandes, J., Saudubray, M., van den Berghe, G., Walter, J. H., Eds., 5th ed.; Springer: Verlag, Heidelberg, 2011.
3. Berry, G. T. Galactosemia. In: NCBI GeneReviewsTM. University of Washington, Seattle. http://www.ncbi.nlm.nih.gov/books/NBK1518/. Last Update April 3, 2014.
4. Gitzelmann, R. *Eur. J. Pediatr.* **1995**, *154*, S45.
5. Waggoner, D. D.; Buist, N. R.; Donnell, G. N. *J. Inherit. Metab. Dis.* **1990**, *13*, 802.
6. Schweitzer, S.; Shin, Y.; Jakobs, C.; Brodehl, J. *Eur. J. Pediatr.* **1993**, *152*, 36.
7. Waisbren, S. E.; Potter, N. L.; Gordon, C. M.; Green, R. C.; Greenstein, P.; Gubbels, C. S.; Rubio-Gozalbo, E.; Schomer, D.; Welt, C.; Anastasoaie, V.; D'Anna, K.; Gentile, J.; Guo, C. Y.; Hecht, L.; Jackson, R.; Jansma, B. M.; Li, Y.; Lip, V.; Miller, D. T.; Murray, M.; Power, L.; Quinn, N.; Rohr, F.; Shen, Y.; Skinder-Meredith, A.; Timmers, I.; Tunick, R.; Wessel, A.; Wu, B. L.; Levy, H.; Elsas, L.; Berry, G. T. *J. Inherit. Metab. Dis.* **2012**, *35*, 279.
8. Donnell, G. N.; Bergren, W. R.; Perry, G.; Koch, R. *Pediatrics* **1963**, *31*, 802.
9. Webb, A. L.; Singh, R. H.; Kennedy, M. J.; Elsas, L. J. *Pediatr. Res.* **2003**, *53*, 396.
10. Guerrero, N. V.; Singh, R. H.; Manatunga, A.; Berry, G. T.; Steiner, R. D.; Elsas, L. J. *J. Pediatr.* **2000**, *137*, 833.
11. Robertson, A.; Singh, R. H.; Guerrero, N. V.; Hundley, M.; Elsas, L. J. *Genet. Med.* **2000**, *2*, 142.
12. Bosch, A. M.; Bakker, H. D.; van Gennip, A. H.; van Kempen, J. V.; Wanders, R. J. A.; Wijburg, F. A. *J. Inherit. Metab. Dis.* **2002**, *25*, 629.
13. Wierenga, K. J.; Lai, K.; Buchwald, P.; Tang, M. *J. Biomol. Screening* **2008**, *13*, 415–423.
14. Odejinmi, S. I.; Rascon, R. G.; Tang, M.; Vankayalapati, H.; Lai, K. *ACS Med. Chem. Lett.* **2011**, *2*, 667.
15. Boxer, M. B.; Shen, M.; Tanega, C.; Tang, M.; Lai, K.; Auld, D. S. Probe Reports from the NIH Molecular Libraries Program [Internet]. Bethesda (MD): National Center for Biotechnology Information (US); 2010 Mar 18. updated 2011 Mar 3.
16. Potapov, A. Y.; Shikhaliev, Kh. S.; Krylsky, D. V.; Krisin, M. Yu. *Chem. Heterocycl. Compd.* **2006**, *42*, 1338.